supplementary information

Flexible, Transparent and Highly Sensitive SERS Substrates with Cross-nanoporous Structures for Fast On-site Detection

Yingcheng Wang[1,2], Yuanhao Jin[1,2], Xiaoyang Xiao[1,2], Tianfu Zhang[1,2], Haitao Yang[1,2], Yudan Zhao[1,2], Jiaping Wang[1,2], Kaili Jiang[1,2], Shoushan Fan[1,2], and Qunqing Li[1,2]*

[1]State Key Laboratory of Low-Dimensional Quantum Physics, Department of Physics & Tsinghua-Foxconn Nanotechnology Research Center, Tsinghua University, Beijing 100084, China

[2]Collaborative Innovation Center of Quantum Matter, Beijing, China

*Corresponding author. E-mail address: qunqli@mail.tsinghua.edu.cn

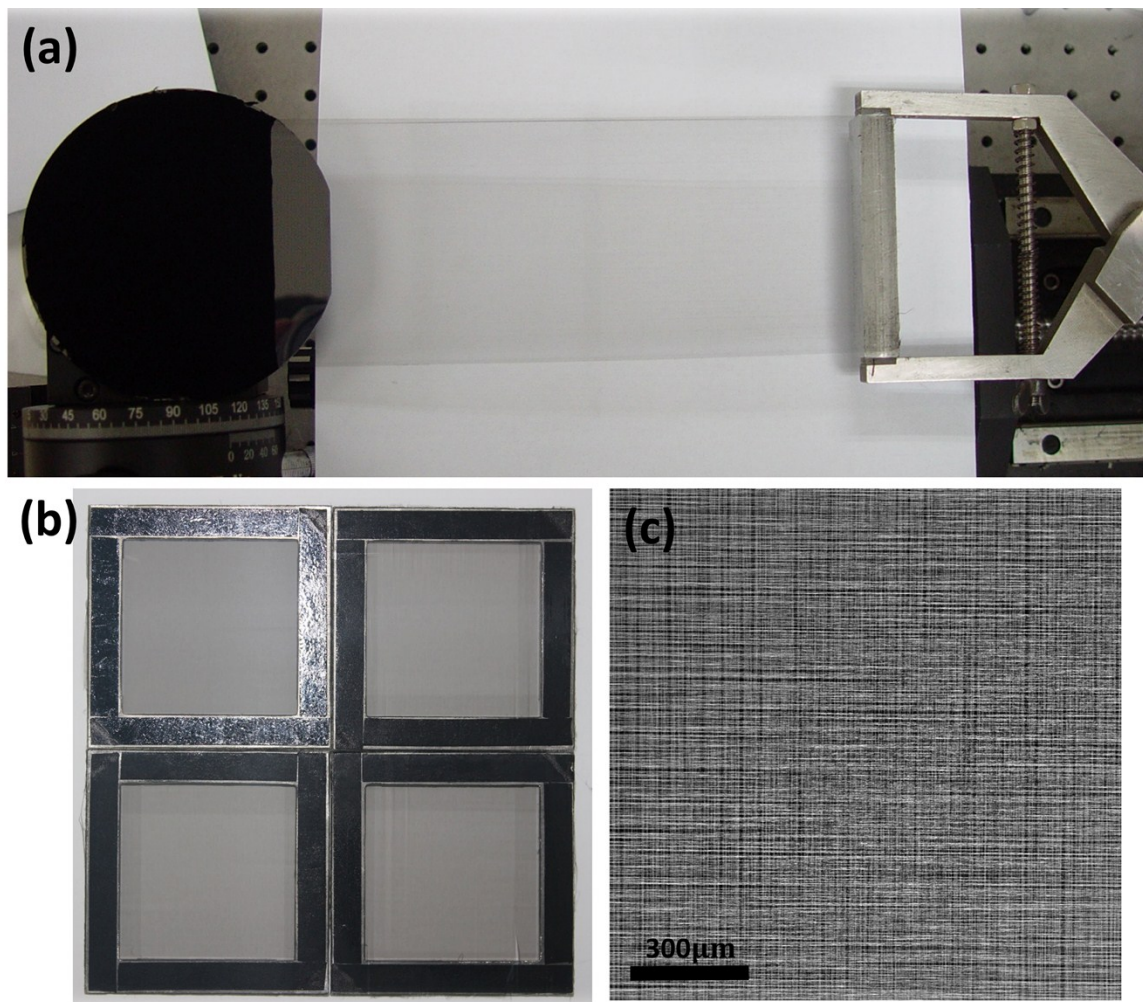## 1. Preparation and characterization of pure SACNT films.

Figure S1. (a) The pure SACNT films can be continuously drawn from super-aligned carbon nanotube arrays under dry conditions. (b) The suspended SACNT films cross-stacked on four metal frames. (c) SEM image of the suspended SACNT networks with a quasi-periodic pattern over a large-scale area.

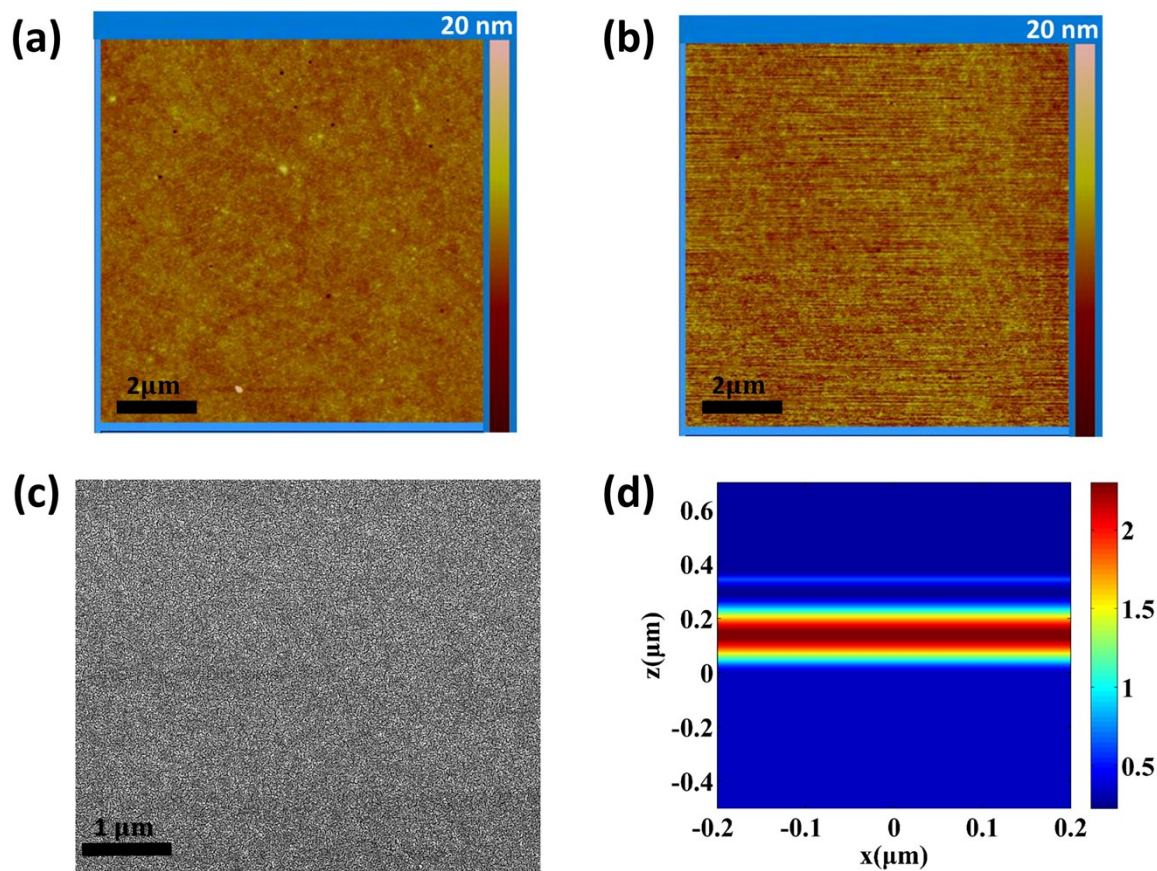## 2. Morphology characterization and finite difference time domain (FDTD) simulation of 10 nm Au@PET.

Figure S2. (a) AFM image of the PET with a surface roughness of $R_a \sim 0.5$ nm. (b) AFM and (c) SEM image of 10 nm unpatterned gold on PET film. (d) Simulated intensity distribution of the local electromagnetic field in the XZ profile of 10 nm unpatterned gold on PET film.

3. Cross-nanoporous model and results of ~~finite difference time domain~~ (FDTD) simulations.

To investigate the interactions of the electromagnetic field with the cross-nanoporous structures (CNS) with Au nanoparticles, finite difference time domain (FDTD) simulations were carried out to calculate the local electromagnetic field distribution. In the simulations, a simplified ideal unit model with Au nanoparticles around the SiO_2 grid was constructed, as shown in Figure S3(a) and (c). The period along the two orthogonal directions of the grid are adopted as 300 nm and the line width of SiO_2 is ~100 nm, according to our SEM observations. The depth of the CNS of SiO_2 is 250 nm, and the radius of the Au nanoparticles is set as 24 nm with a spacing of 2 nm between them. The calculations were performed under the perpendicular irradiation of a laser with wavelength of 632.8 nm, from the front side and back side of the model, respectively. The dielectric permittivity of PET was ε=3.901+i*0.003, while those of bulk Au and SiO_2 were based on experimental results of previous works.[1,2] The amplitude of the incident electromagnetic (EM) field was set as 1 V m^{-1} with polarization set parallel to one direction of the SiO_2 grid.

Figure S3(b) and (d) shows the calculated intensity distribution of the normalized local electromagnetic field near the cross-nanoporous structures with Au nanoparticles, under front-side and back-side irradiation. It is clear that the total EM field is significantly enhanced by a high density of "hot spots" generated from nanogaps and sharp edges, where an extraordinarily large EM field enhancement depicted by a factor of $(\frac{E}{E_0})^2$ can be seen on the CNS with Au nanoparticles. Furthermore, the maximal EM field enhancement factor for the front-side mode is about 3.4×10^3, and appears on the top surface of the structures by a rigorously simulation and

analyzation. While for that of the back-side mode it can reach 1.6×10^4, which appears in the grooves of the CNS of Au. The calculated results confirm that Raman signals of probe molecules can be largely enhanced by exciting the LSP of Au nanoparticles formed on the reverse of the substrate in back-side mode, which are in consistence with the experimental results. For comparison, the simulated intensity distribution of the local electromagnetic field of 10nm Au@PET is also shown in Figure S2(d), with maximal EM field enhancement factor of ~2.5.
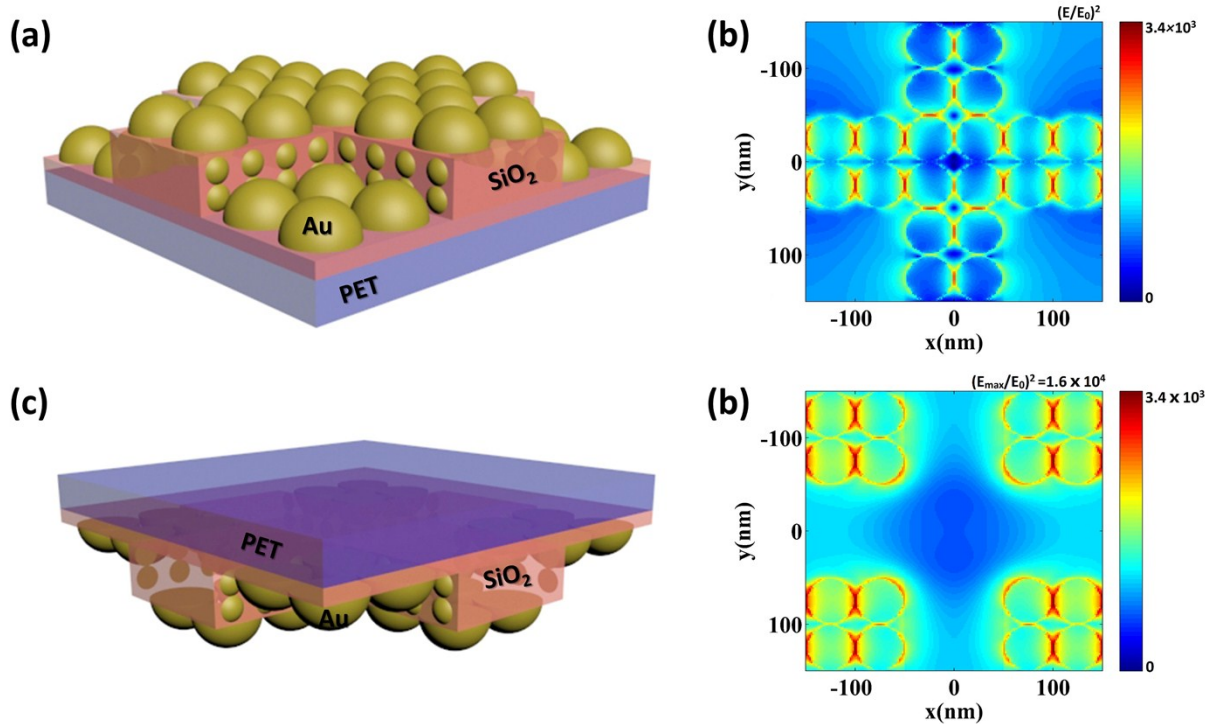

Figure S3. A simplified ideal unit model for FDTD simulations with (a) front-side mode and (c) back-side mode. Calculated intensity distribution of the local electromagnetic field near the cross-nanoporous structures with Au nanoparticles irradiated by (b) front side and (d) back side.

4. Effect of mechanical bending on the SERS performance of flexible substrates.

To verify the SERS responses to cyclic mechanical effect on the flexible substrate with an induced bending strain, the SERS performance of resulting substrate was performed and compared after five bending cycles at a radius of less than 3 mm, as shown in Figure S4. Two different concentrations (10^{-6} M and 10^{-8} M) of CV ethanol solution were dropped onto the substrates before and after five bending cycles, respectively, from which we can see that the enhanced Raman intensity was almost the same after five bending cycles. It demonstrates that the appropriate bending strains have little influence on the excitation of "hot spots" from narrow metal nanogaps and sharp edges, which sustain the sensitivity of the flexible SERS substrate. Therefore, the as-fabricated substrate is acceptable to use it as an efficient flexible SERS sensor.
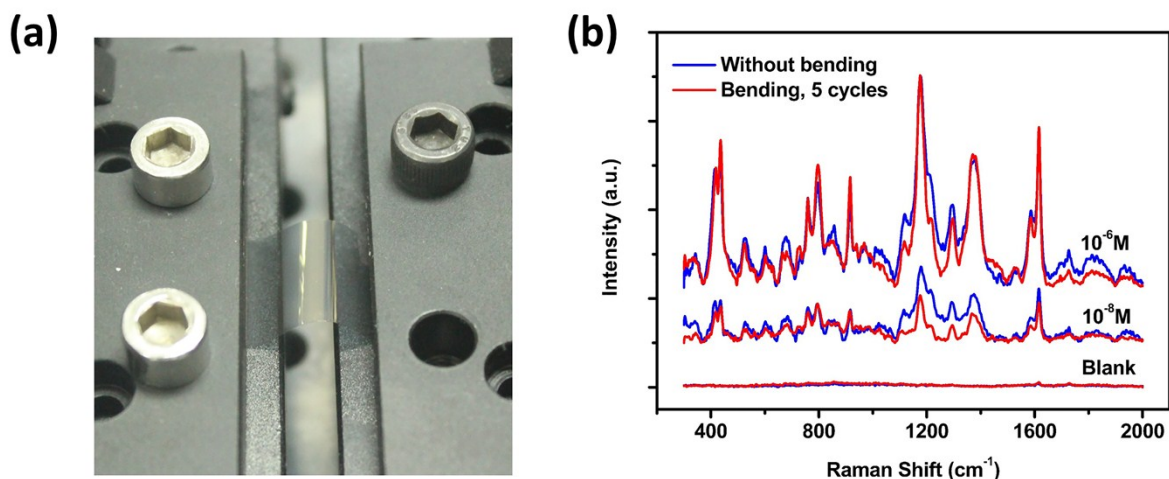

Figure S4. (a) Bending control of the flexible SERS substrate by an automatic machine. (b) SERS spectra of CV, collected from the flexible SERS substrates before and after five bending cycles at a radius of less than 3 mm, with analyte concentrations of 10^{-6} and 10^{-8} M dropped onto their surface. The exposure time was 5 s.

5. Vibrational assignments of Raman bands in SERS spectra for different analytes.

TABLE S1. Band assignments of the partial characteristic peaks in the Raman spectrum of Figure 3(c) to vibrational modes of Crystal Violet and Polyethylene Terephthalate.

Crystal Violet (CV)		Polyethylene Terephthalate (PET)	
Raman Shift [1]	Band assignments [2]	Raman Shift [a]	Band assignments [3]
436	Ph-C-Ph bend	631	C-C-C in plane bend
798	Ring C-H bend	858	C-C breathing
915	Ring skeletal vib. Of radical orientation	1286	Ring and C-O stretching
1176	Ring C-H bend	1612	Ring C-C stretching
1296	Ring C-C stretching	1726	C-O stretching
1374	N-phenyl stretching		
1587	Ring C-C stretching		
1620	Ring C-C stretching		

[1] Units in wavenumber (cm^{-1}).

[2] The band assignments were on the basis of references 3 and 4.

[3] The band assignments were on the basis of references 5 and 6.

TABLE S2. Band assignments of the partial characteristic peaks in the Raman spectrum of Figure 6 to vibrational modes of 4-aminothiophenol.

4-aminothiophenol (4-ATP)	
Raman Shift [1]	Band assignments [2]
1006	C-C-C and C-C bend
1076	C-S stretching
1138	Ring C-H bend
1183	Ring C-H bend
1388	C-C stretching and C-H bend
1435	C-C stretching and C-H bend
1571	Ring C-C stretching

[1] Units in wavenumber (cm^{-1}).

[2] The band assignments were on the basis of references 7 and 8.

6. SERS detection of thiram pesticides using the flexible SERS substrate with a swabbing technique.
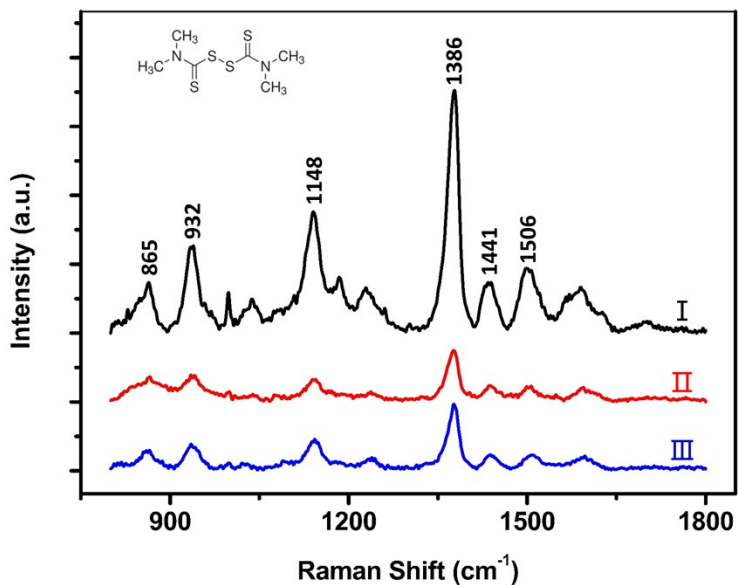

Figure S5. SERS spectra of Thiram pesticides collected from the resultant flexible substrate: (I), (II) after being immersed in Thiram ethanol solutions with concentrations of 10^{-5} M (black curve) and 10^{-7} M (red curve) for 1 h; (III) after swabbing the apple skin applied with 10^{-5} M Thiram solution. The exposure time was 20 s.

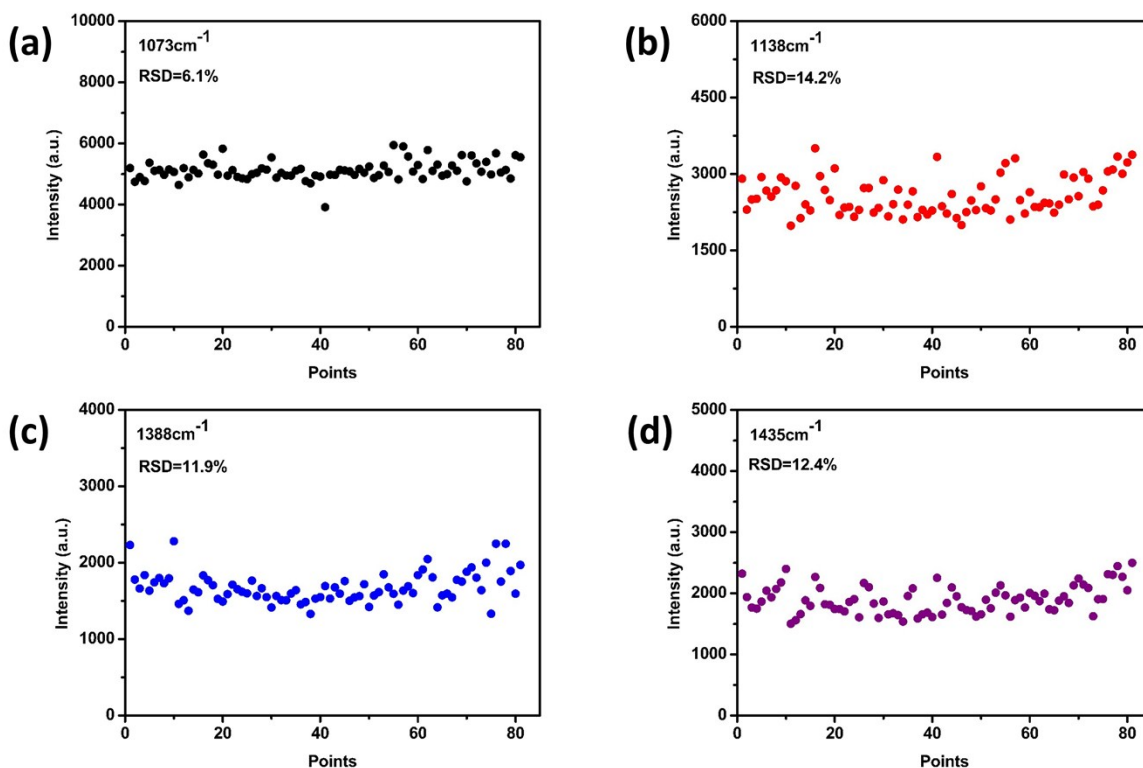**7. The intensity distribution of several vibrational bands of 4-ATP with a corresponding calculated RSD.**

Figure S6. The intensity distribution of 10^{-6} M 4-ATP at the vibrational bands at 1073, 1138, 1388 and 1435 cm^{-1} with corresponding RSD of 6.1%, 14.2%, 11.9% and 12.4%, respectively.

Notes and references

1   P. B. Johnson, R. W. Christy, *Phys. Rev. B*, 1972, **6**, 4370-4379.

2   E. D. Palik, *Handbook of Optical Constants of Solids*, Academic Press, San Diego, 1985.

3   E. J. Liang, X. L. Ye, W. Kiefer, *J. of Phys. Chem. A*, 1997, **101**, 7330-7335.

4   L. Zhang, X. Lang, A. Hirata, M. Chen, *ACS Nano*, 2011, **5**, 4407-4413.

5   T. Lippert, F. Zimmermann, A. Wokaun, *Appl. Spectrosc.*, 1993, **47**, 1931-1942.

6   J. Purvis, D. I. Bower, J. Polym., *Sci. Pol. Phys.*, 1976, **14**, 1461-1484.

7   K. Kim, J. K. Yoon, *J. Phys. Chem. B*, 2005, **109**, 20731-20736.

8   K. Uetsuki, P. Verma, T. A. Yano, Y. Saito, T. Ichimura, S. Kawata, *J. Phys. Chem. C*, 2010, **114**, 7515-7520.